

Fast and robust quantum computation with ionic Wigner crystals

J. D. Baltrusch^{1,2,3}, A. Negretti¹, J. M. Taylor⁴ and T. Calarco^{1,5}

¹*Institute for Quantum Information Processing, University of Ulm,
Albert-Einstein-Allee 11, D-89069 Ulm, Germany*

²*Grup d'Òptica, Edifici CC, Universitat Autònoma de Barcelona (UAB), E-08193 Bellaterra (Barcelona), Spain*

³*Theoretische Physik, Universität des Saarlandes, 66041 Saarbrücken, Germany*

⁴*Joint Quantum Institute and the National Institute of Standards and Technology, College Park, Maryland 20742, USA*

⁵*Department of Physics, Harvard University, and ITAMP, Cambridge, MA 02138, USA*

(Dated: April 19, 2011)

We present a detailed analysis of the modulated-carrier quantum phase gate implemented with Wigner crystals of ions confined in Penning traps. We elaborate on a recent scheme, proposed by two of the authors, to engineer two-body interactions between ions in such crystals. We analyze for the first time the situation in which the cyclotron (ω_c) and the crystal rotation (ω_r) frequencies do not fulfill the condition $\omega_c = 2\omega_r$. It is shown that even in the presence of the magnetic field in the rotating frame the many-body (classical) Hamiltonian describing small oscillations from the ion equilibrium positions can be recast in canonical form. As a consequence, we are able to demonstrate that fast and robust two-qubit gates are achievable within the current experimental limitations. Moreover, we describe a realization of the state-dependent sign-changing dipole forces needed to realize the investigated quantum computing scheme.

PACS numbers: 03.67.Lx, 37.10.Ty, 37.10.De, 45.50.-j

I. INTRODUCTION

Despite the huge experimental progress to cool, trap, and manipulate single particles such as atoms and molecules at the quantum level, the way to build up a quantum computing hardware working with several hundreds of quantum bits (qubits) in a coherent and controllable manner is still long. By means of quantum optimal control techniques it is possible, at least theoretically, to perform one- and two-qubit quantum gates with fidelities above the demanding thresholds of fault-tolerant quantum computation [1–9]. These thresholds fix an error between 0.01% to fractions of a percent [10, 11]. Up to now, only with cold trapped ions quantum gates with a fidelity of 99.3% have been experimentally demonstrated [12, 13], which is not too far from the aforementioned thresholds. Similar fidelities have been also obtained for small quantum algorithms [14, 15].

Nowadays, however, most of the experimental efforts of the atomic and molecular physics community are concentrated in the design and fabrication of microtraps, both for ions [16, 17] and neutral atoms [18, 19]. Even though these efforts are important, significant technical issues related to the miniaturization and trapping methodologies arise when scaling to many particles, and therefore new strategies have to be devised. A possible solution to the problem is the separation between the qubits used as quantum memory and the ones employed to process the information [20] or, alternatively, the exploitation of quantum distributed networks [21]. Another approach, instead, consists in the use of collective states of atomic ensembles with a multilevel internal structure as qubits [22].

Apart from these technological efforts and alternative solutions, nobody can yet say which of the various phys-

ical implementations will be the successful one. It is fair to say, however, that ions represent a good candidate to implement a multi-qubit quantum processor. Indeed, two-qubit gates with ions can be realized in about few tens of μs [23, 24], and qubits stored in internal electronic degrees of freedom of an ion have coherence lifetimes ranging from 1 s to 100 s or more [24].

Coulomb — also named classical Wigner — crystals confined in Penning traps are natural candidates for a quantum memory, since the separation among ions, about 10 μm , allows to individually manipulate their internal degrees of freedom. Such a trap scheme uses static electric fields to confine charge particles in the axial direction (the z axis in Fig. 1), whereas the radial confinement is provided by a strong uniform magnetic field along the axial direction. Currently, Penning traps allow to trap up to 10^8 ions [25]. An appropriate choice of the trap parameters (e.g., tight axial confinement) allows the ionic ensemble to crystallize in a two-dimensional (2D) hexagonal lattice configuration with an inter-particle spacing on the order of tens of μm [26], and therefore to manipulate a large number of qubits without specific micro-trap designs. The high phonon mode density, however, does not permit to resolve single modes for sideband cooling. Hence, Doppler and sympathetic cooling are the most natural techniques to be employed; we also note that Sisyphus cooling might be an alternative methodology [27]. Current experiments, however, performed with Doppler cooling, can reach temperatures of few mK [28], that is, a high thermal occupation number distribution of phonon modes. Nonetheless, efficient quantum computation and production of small cluster states are theoretically possible [29, 30], and recently full control of the qubit Bloch vector with $\sim 99.85\%$ fidelity for Rabi flopping has been experimentally demonstrated [31].

The two-qubit gate scheme considered in the propos-

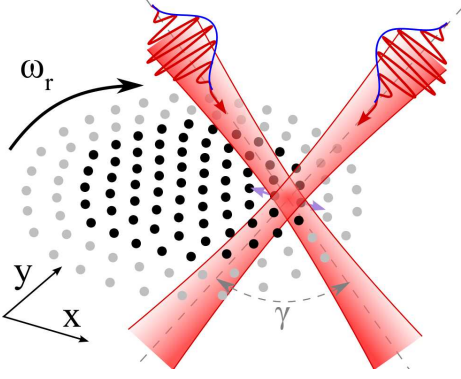


FIG. 1. (Color online). Two-dimensional Coulomb crystals of ions in a Penning trap rotating at frequency ω_r . To manipulate the internal states of the ions, laser beams can address single sites or multiple ions.

als of Refs. [29, 30] is based on the so called “pushing gate” (or its variant, the modulated-carrier gate), where a spatially inhomogeneous laser field together with an appropriate combination of polarizations and frequencies induces a state-dependent dipole force on two nearest neighbours of the 2D Coulomb crystal (see Fig. 1). Depending on the configuration of lasers and polarizations the displacements of the ions away from their equilibrium positions can be either perpendicular to the plane of the crystal [29] or along the in-plane separation of the ions [30, 32–34]. The coupling between these displacements, mediated by phonons, yields entanglement of the internal states (qubits) of the ions, that is, the desired quantum gate between ions.

In addition to the confinement, the radial electric and axial magnetic fields induce a drift that causes in-plane rotation of the crystal (see Fig. 1), whose frequency $\omega_r/(2\pi)$ is typically on the order of few tens of kHz [26]. There are two possible solutions to our quantum hardware design: either we use a co-rotating (with the crystal) laser beam in order to realize the desired two-qubit quantum gate, or we have to perform the gate in a time, τ_g , such that the crystal rotation has a negligible effect on the gate operation. The latter solution translates in the condition $\omega_r\tau_g/(2\pi) \ll 1$. Such a requirement is instrumental because, in order to accumulate the necessary two-ion phase for the quantum gate we aim to implement, the ions have to experience the applied light force for the entire gate operation, or else, the required phase would be achieved only partially.

While the former solution applies for all rotation frequencies, but relies on a more sophisticated experimental setup, the latter restricts the range of possible values of ω_r . Thus, in both proposals [29, 30], where the rotation and cyclotron frequencies fulfill $2\omega_r = \omega_c$, the aforementioned condition is satisfied when τ_g is on the order of ns, whereas the modulated-carrier gate of Ref. [30] had $\tau_g = 5 \mu\text{s}$. Given the above, such a proposal requires a

co-rotating laser beam. Thus, by maintaining $2\omega_r = \omega_c$ one should reduce ω_c . This approach, however, would not help since the smaller the cyclotron frequency is, the longer the gate operation. Instead, if we abandon the assumption $2\omega_r = \omega_c$ and look at moderate rotation frequencies, at the expenses of possible large modulations of the force, we are able to fulfill $\omega_r\tau_g/(2\pi) \ll 1$. Additionally, low rotating frequencies result in low densities and large inter-particle spacing, and therefore in an easier way to address the trapped ions with a laser field.

Thus, the main goal of this work is to analyze this regime and, at the same time, to perform robust two-qubit gates within a range of experimentally achievable temperatures.

In the following we shall present the general theory of the modulated-carrier push two-qubit gate (Sec. II) with details that were briefly mentioned in Ref. [30]. Subsequently, in Sec. III, we investigate the situation in the presence of the magnetic field in the rotating frame of reference and the relative gate performance. In section IV we describe how to physically realize the state-dependent force required for the proposed quantum processor, and Sec. V summarizes our results and provides some future perspectives.

II. MODULATED-CARRIER GATE

In the following we make the approximation that the Wigner crystal is a rigid body, which is a good approximation in the magnetohydrodynamic regime (one component plasma) or at equilibrium [35]. Hence, in a rotating frame, the Hamiltonian of a crystal with N ions written in cylindrical coordinates $[\vec{r} \equiv (r, \theta, z)]$ is given by [35]

$$H_R(\omega) = \sum_{k=1}^N \left\{ \frac{p_{r_k}^2 + p_{z_k}^2}{2m} + \frac{[p_{\theta_k} - m(\omega_c - 2\omega)r_k^2/2]^2}{2mr_k^2} \right\} + \sum_{k=1}^N \left\{ \Upsilon(2z_k^2 - r_k^2) + \frac{m}{2}\omega(\omega_c - \omega)r_k^2 \right\} + V_c, \quad (1)$$

with m being the mass of the ion and

$$V_c = \frac{e^2}{4\pi\epsilon_0} \sum_{k < j} \frac{1}{|\vec{r}_k - \vec{r}_j|}. \quad (2)$$

Here Υ is a parameter describing the trap geometry and applied voltage on the electrodes [36], ϵ_0 the vacuum permittivity, e the electron charge, and $\omega_c = eB/m$ is the cyclotron frequency. We see, from the first line of Eq. (1), that there exists a special rotating frame, $\omega = \omega_c/2$, such that the minimal coupling disappears, and, in this section, we shall consider such a frame of reference together with $\omega_r = \omega_c/2$ (i.e., the frame of reference coincides with the crystal). We note, that with “minimal coupling” we

refer to the interaction $\vec{p} \cdot \vec{A}$. Such terminology is typically used in quantum field theory [37].

Finally, it is worth to remind that the gate we aim to accomplish realizes the true table $|\epsilon_1, \epsilon_2\rangle \rightarrow e^{i\theta\epsilon_1\epsilon_2} |\epsilon_1, \epsilon_2\rangle$ with $\epsilon_{1,2} = 0, 1$ and $\theta = \theta_{00} - \theta_{01} - \theta_{10} + \theta_{11}$ [33, 34]. Specifically, we are interested in a phase gate with $\theta = \pi$, which, up to additional single-qubit rotations, is tantamount to a two-qubit controlled NOT gate [24].

A. Normal modes and canonical quantization

The Hamiltonian (1) in cartesian coordinates $[\vec{r} \equiv (x, y, z)]$ reduces to

$$H_R\left(\frac{\omega_c}{2}\right) = \sum_{k=1}^N \left\{ \frac{\vec{p}_k^2}{2m} + \frac{m}{2} [\omega_z^2 z_k^2 + \omega_{xy}^2 (x_k^2 + y_k^2)] \right\} + V_c, \quad (3)$$

where $\omega_z = \sqrt{4\Upsilon/m}$ is the axial frequency, and $\omega_{xy} = 1/2(\omega_c^2 - 2\omega_z^2)^{1/2}$ the in-plane one.

By performing a Taylor expansion of the potential up to second order around the stable equilibrium configuration, obtained by minimizing the total crystal energy, we can express the Hamiltonian in the new coordinates $q_{n,\eta} \equiv \eta_n - \eta_n^0$, that is, the displacements from the equilibrium positions. Hence, it is possible to determine an orthogonal transformation M such that¹

$$H_R\left(\frac{\omega_c}{2}\right) \approx \sum_{n,\eta} \left\{ \frac{P_{n,\eta}^2}{2m} + \frac{m}{2} \omega_{n,\eta}^2 Q_{n,\eta}^2 \right\} \quad (4)$$

with $Q_{n,\eta} = \sum_{k,\mu} M_{n,\eta;k,\mu} q_{k,\mu} [= M\mathbf{q}]$, and $P \equiv p$.

Now, we perform the canonical quantization and we introduce the creation (annihilation) operators \hat{a}_K^\dagger (\hat{a}_K) for each mode $K \equiv (n, \eta)$, along with the harmonic oscillator ground state size $\alpha_K = \sqrt{\hbar/m\omega_K}$. Hence, the (phononic) Hamiltonian operator reads

$$\hat{H}_R = \sum_K \hbar\omega_K (\hat{a}_K^\dagger \hat{a}_K + 1/2), \quad (5)$$

where for the sake of simplicity we drop $(\frac{\omega_c}{2})$ in \hat{H}_R .

B. Adiabatic and oscillatory quantum gates

Let us consider a spatially inhomogeneous laser field appropriately detuned from the internal states such that

it produces a state-dependent displacement of the ions. Then, the matter-field interaction, in the electric dipole approximation, becomes

$$\hat{V} = \sum_{j=1}^N [\hat{q}_j \cdot \vec{f}_j(t)] \hat{\sigma}_j^z = \sum_K \frac{\alpha_K}{\sqrt{2}} \hat{f}_K(t) (\hat{a}_K^\dagger + \hat{a}_K), \quad (6)$$

where \vec{f}_j is the three dimensional force due to the gradient in the laser intensity, and $\hat{\sigma}_j^z$ is the z Pauli matrix. Here the following relation for the displacement coordinate operator

$$\hat{q}_K = \sum_{K'} M_{K',K} \hat{Q}_{K'} = \sum_{K'} M_{K',K} \frac{\alpha_{K'}}{\sqrt{2}} (\hat{a}_{K'} + \hat{a}_{K'}^\dagger) \quad (7)$$

has been used. Thus, we have $[K \equiv (j, \mu)]$

$$\hat{f}_K(t) = \sum_{j',\mu'} M_{K;j',\mu'} [\vec{f}_{j'}(t)]_{\mu'} \hat{\sigma}_{j'}^z, \quad (8)$$

where $[\vec{f}_{j'}(t)]_{\mu'}$ is the $\mu' = x, y, z$ component of the three-dimensional vector $\vec{f}_{j'}(t)$. Hence, the full problem reduces to $3N$ independent, driven oscillators.

When the temporal profile of the force fulfills the condition $\lim_{t \rightarrow \pm\infty} f(t) = 0$, the unitary time evolution operator is given by $\hat{U}_K(t) = e^{-i\phi_K(t)} \exp(\beta_K \hat{a}_K^\dagger - \beta_K^* \hat{a}_K) \exp(-i\omega_K t \hat{a}_K^\dagger \hat{a}_K)$, where ϕ_K and β_K satisfy the differential equations [38, 39]

$$\dot{\beta}_K = -i\omega_K \beta_K + i \frac{\alpha_K}{\hbar\sqrt{2}} \hat{f}_K(t), \quad \dot{\phi}_K = \frac{\alpha_K}{\hbar\sqrt{2}} \hat{f}_K(t) \text{Re}[\beta_K(t)]. \quad (9)$$

Given that, let us consider the adiabatic regime regime where $\hat{f}_K(t)$ varies slowly with respect to ω_K [33]. Adiabatic elimination, by taking $\dot{\beta}_K \rightarrow 0$, yields

$$\beta_K \approx \frac{\alpha_K \hat{f}_K(t)}{\hbar\omega_K \sqrt{2}}, \quad \dot{\phi}_K \approx \frac{\alpha_K^2 \hat{f}_K^2(t)}{2\hbar^2 \omega_K}. \quad (10)$$

Thus, the displacement of a normal mode K induced by the gate is proportional to the force applied, and can be made zero independent of the initial phonon state by starting and ending with zero force. This eliminates any potential error due to entanglement between phonons and the internal states of the ions. Similarly, the overall phase accumulated $\sum_K \phi_K(\tau_g)$ does not depend on the initial phonon state. However, for a gate occurring over a time interval $[0, \tau_g]$, the final qubit state has applied $\exp(-i \sum_{nj} \phi_{nj} \hat{\sigma}_n^z \hat{\sigma}_j^z)$, where the two-particle phases arise from

$$\hat{f}_K^2(t) = \sum_{j,n;\mu,\eta} M_{K;j,\mu} M_{K;n,\eta} [\vec{f}_j(t)]_\mu [\vec{f}_n(t)]_\eta \hat{\sigma}_j^z \hat{\sigma}_n^z. \quad (11)$$

¹ Hereafter we shall use latin symbols for index the ions and greek symbols for the cartesian coordinate of the force vector acting on the ions.

Thus, the two-particle phase is given by

$$\phi_{nj} = \sum_{\mu,\eta} S_{\mu\eta}^{(nj)} \int_0^{\tau_g} dt [\vec{f}_j(t)]_\mu [\vec{f}_n(t)]_\eta, \quad (12)$$

where the term outside the integral is a shape independent form factor, whose specific form is given by

$$S_{\mu\eta}^{(nj)} = \sum_K \frac{\alpha_K^2}{2\hbar^2\omega_K} M_{K;j,\mu} M_{K;n,\eta}. \quad (13)$$

Hence, we can think about (12) as a convolution of the forces on the two particles, modified by the form factor representative of the characteristic oscillator variance over its frequency, which is overall proportional to ω_K^{-1} .

Now, let us consider a scheme with a force $f(t) \rightarrow \cos(\nu t)f(t)$, where the carrier frequency ν must be much larger than the modes of frequency ω_K that are coupled to the force (this averages out any net displacement). If the modulation $f(t)$ is slow as compared to ν (but with no restriction with respect to ω_K), we can perform a similar adiabatic elimination as above, and get a gate with the same desirable properties that can operate non-trivially on arbitrarily in-plane vibrational modes at very high temperatures.

For adiabatic elimination with respect to ν , we choose the Ansatz $\beta_K = \beta_K^+ e^{i\nu t} + \beta_K^- e^{-i\nu t}$ for each mode. By inserting this Ansatz into the differential equation (9) we obtain

$$\begin{aligned} \dot{\beta}_K^+ = e^{-2i\nu t} & \left[i \frac{\alpha_K}{2\sqrt{2}\hbar} \hat{f}_K(t) - \dot{\beta}_K^- - i(\omega_K - \nu)\beta_K^- \right] \\ & + i \frac{\alpha_K}{2\sqrt{2}\hbar} \hat{f}_K(t) - i(\omega_K + \nu)\beta_K^+. \end{aligned} \quad (14)$$

Separate adiabatic elimination of β_K^- and β_K^+ yields $\beta_K^\pm = \alpha_K \hat{f}_K(t) / [2\sqrt{2}\hbar(\omega_K \pm \nu)]$. As before, in the pure adiabatic regime, we find that the displacement of a normal mode induced by the gate is proportional to the force applied. Again, it can be made zero independent of the initial phonon state by starting and ending with zero force, and therefore eliminating any potential error due to entanglement between phonons and the internal states of the ions.

Now, we examine the two-particle phase induced in this new scenario. The time evolution of the phase is governed by [30]

$$\dot{\phi}_K = \frac{\alpha_K^2}{2\hbar^2} \frac{\omega_K}{(\omega_K^2 - \nu^2)} \cos^2(\nu t) \hat{f}_K^2(t), \quad (15)$$

where the quickly varying component $\cos^2(\nu t)$ can be replaced with $1/2$. As described in the adiabatic regime, the overall phase accumulated $\sum_K \phi_K(\tau_g)$, for a gate occurring over a time interval $[0, \tau_g]$, does not depend on

the phonon initial state. In this case the pulse-shape independent form factor is given by [30]

$$S_{\mu\eta}^{(nj)} = - \sum_K \frac{\alpha_K^2 \omega_K}{4\hbar^2(\nu^2 - \omega_K^2)} M_{K;j,\mu} M_{K;n,\eta}. \quad (16)$$

Performing a Taylor expansion in $1/\nu^2$ the first term is proportional to $\sum_K M_{K;j,\mu} M_{K;n,\eta} = \delta_{j,n} \delta_{\mu,\eta}$ ($\delta_{j,n}$ indicates the Kronecker symbol). This follows from the fact that M is an orthogonal matrix. Physically, this arises due to the coherent averaging of in-phase oscillating ions without any virtual excitation of phonons—accordingly, no two-body phase should be expected. The second term of the expansion is non-zero and yields

$$\tilde{S}_{\mu\eta}^{(nj)} = - \frac{1}{4\hbar m \nu^4} \sum_K \omega_K^2 M_{K;j,\mu} M_{K;n,\eta} + O(\nu^{-6}). \quad (17)$$

Compared to adiabatic push gates, the modulated-carrier gate is inverted in sign and it is multiplied (in phase) by a factor $(\omega_K/\nu)^4/2$ [see Eq. (13)]. In the case of a lateral operating modulated-carrier gate with $\omega_{xy} \ll \nu \ll \omega_z$, the accumulated phase is enhanced by a factor $(\omega_z/\nu)^4/2$ with respect to an adiabatic push gate with a force moving the ions in the axial (z) direction for the same laser parameters. Given that, the gate time needed to perform a π -phase gate is reduced. In the opposite case, that is, for an adiabatic in-plane push gate ($\omega_K \sim \omega_{xy}$), and for the same laser parameters, the lateral modulated-carrier gate is reduced in phase, and therefore a longer τ_g is required. Thus, compared to the proposal of Ref. [29], where the push gate operates in the axial direction, our modulated-carrier gate working with in-plane modes yields a larger two-ion phase for a given set of laser parameters, and therefore it enables to perform a larger number of quantum gates within the coherence time of the system.

III. MODULATED-CARRIER GATE WITH MINIMAL COUPLING

In this section we analyze the situation where $\omega_r \neq \omega_c/2$, for which we have three reasonable choices for the rotating frame of reference:

- F_1 coincides with the lab frame, where the equilibrium positions of the ions in the crystal are time-dependent and the minimal coupling does not vanish;
- F_2 rotates with a frequency $\omega = \omega_c/2$, as in the previous section, where the minimal coupling vanishes, but the equilibrium positions are time-dependent;
- F_3 rotates with a frequency $\omega = \omega_r$, where equilibrium positions are time-independent, but the minimal coupling does not vanish.

A. Equilibrium configuration of the crystal

Let us discuss which of the frames of reference $F_{1,2,3}$ is more suitable to numerically determine the equilibrium configuration of the system for a fixed (a priori) value of total canonical angular momentum P_θ ². Since we are not concerned with relativistic velocities, the electromagnetic fields involved in the problem are the same in all frames of reference. Consequently, the angular momentum of an ion in a frame rotating with uniform angular velocity with respect to the (inertial) laboratory frame coincides with the one in the latter [40]. This conclusion allow us to find the equilibrium configuration of the crystal, for a given value of P_θ , by choosing a frame of reference rotating with angular velocity $\omega = \omega_c/2$ (the frame F_2 in the above outlined list) in such a way that the coordinate systems at the initial time $t = 0$ of F_2 and F_3 do coincide. Such a choice simplifies the numerical minimization procedure, because the minimal coupling in the (classical) Hamiltonian vanishes. We underscore, however, that F_2 is utilized only at time $t = 0$ for the determination of the equilibrium configuration of the crystal. Instead, for times $t > 0$ we use F_3 , where the equilibrium positions are time-independent. With such a choice the numerical effort in order to assess the gate performance is significantly reduced.

Besides this, we also note that not all rotation frequencies ω_r of the crystal allow to have a stable configuration, that is, ions confined within a well-defined spatial region. Indeed, by rewriting the addend of the second sum in Eq. (1) as

$$\Upsilon(2z_k^2 - r_k^2) + \frac{m}{2}\omega_r(\omega_c - \omega_r)r_k^2 = \frac{m\omega_z^2}{2}(z_k^2 + \beta r_k^2) \quad (18)$$

we see that the potential is confining if and only if β is positive. Here the anisotropy parameter β is defined as

$$\beta = \frac{\omega_r(\omega_c - \omega_r)}{\omega_z^2} - \frac{1}{2} = \frac{\omega_r}{\alpha_z^2\omega_c} \left(1 - \frac{\omega_r}{\omega_c}\right) - \frac{1}{2}, \quad (19)$$

where $\alpha_z = \omega_z/\omega_c$. Importantly, β relies only on α_z and the ratio ω_r/ω_c . Thus the range of admissible frequencies is: $\omega_m < \omega_r < \omega_c - \omega_m$, where $\omega_m = \omega_c/2 - \omega_{xy}$ is the magneton frequency [35]. Of course, the admissible regime is also constrained by the condition $\alpha_z < 1/\sqrt{2}$. In order to access lower rotation frequencies, the trap parameters might be changed by increasing ω_{xy} , that is, by lowering ω_z . Attention has to be paid, however, when ω_c and ω_z are changed, since due to such a manipulation different structural phase transitions may occur. In particular, we are interested in the limit $\beta \ll 1$, where a 2D hexagonal lattice structure appears [35].

² When $\omega_r \neq \omega_c/2$, the total canonical angular momentum $P_\theta \neq 0$, but it is still a constant of motion [35].

B. Quadratic expansion of the Hamiltonian

Let us introduce the typical scale of length ℓ_s , momentum p_s , and energy E_s in our problem:

$$\ell_s = \left(\frac{e^2}{4\pi\epsilon_0 m\omega_c^2}\right)^{\frac{1}{3}} \quad p_s = \ell_s m\omega_c \quad E_s = \frac{e^2}{4\pi\epsilon_0 \ell_s}. \quad (20)$$

Then, the Hamiltonian (1) in cartesian coordinates becomes

$$\begin{aligned} H_R(\omega) = & \frac{1}{2} \sum_{k=1}^N [p_{x_k}^2 + p_{y_k}^2 + p_{z_k}^2 + (y_k p_{x_k} - x_k p_{y_k}) \times \\ & \times (1 + 2\alpha)] + \frac{1}{4} \sum_{k=1}^N \left[\alpha_z^2 (2z_k^2 - r_k^2) + \frac{r_k^2}{2} \right] \\ & + \frac{1}{2} \lim_{\epsilon \rightarrow 0} \sum_{k,j=1}^N \frac{1 - \delta_{k,j}}{|\vec{r}_k - \vec{r}_j + \epsilon|}, \end{aligned} \quad (21)$$

where the substitutions $H_R(\omega) \rightarrow H_R(\omega)/E_s$, $(r, z) \rightarrow (r, z)/\ell_s$, $(p_x, p_y, p_z) \rightarrow (p_x, p_y, p_z)/p_s$, and $\alpha = \omega/\omega_c$ have been introduced. The expression of the Coulomb potential, third line in Eq. (21), allows to obtain more compact formulae later in the present section.

Next, given the equilibrium configuration $(\vec{r}_0, \vec{0})$ of each ion, we expand the Hamiltonian (21) to second order in the spatial displacement $\mathbf{q} = \mathbf{r} - \mathbf{r}_0$ and \mathbf{p} around zero, namely

$$H_R(\mathbf{p}, \mathbf{q}) \simeq H_R(\mathbf{0}, \mathbf{r}_0) + \frac{1}{2} \mathbf{d} \tilde{H}_R \mathbf{d}^\top, \quad (22)$$

where \mathbf{d}^\top is the transpose of the row vector $\mathbf{d} \equiv (q_{1,x}, p_{1,x}, q_{1,y}, p_{1,y}, \dots, q_{N,z}, p_{N,z})$, and $\tilde{H}_R = \tilde{H}_R(\mathbf{0}, \mathbf{r}_0)$ is the Hessian matrix. Its non-zero matrix elements are given by:

$$\begin{aligned} \frac{\partial^2 H_R}{\partial p_{\eta_k}^2} &= 1, \quad \frac{\partial^2 H_R}{\partial p_{x_k} \partial y_k} = -\frac{\partial^2 H_R}{\partial p_{y_k} \partial x_k} = \alpha + \frac{1}{2}, \\ \frac{\partial^2 H_R}{\partial \eta_k \partial \mu_j} &= [1 - 2\alpha_z^2 + (6\alpha_z^2 - 1)\delta_{\eta,j}] \frac{\delta_{\eta,\mu} \delta_{k,j}}{4} \\ &+ \lim_{\epsilon \rightarrow 0} \sum_{s=1}^N \frac{(1 - \delta_{k,s})[\delta_{s,j} + (1 - \delta_{s,j})\delta_{|k-j|,0}]}{|\vec{r}_k - \vec{r}_s + \epsilon|^3} \times \\ &\times (-1)^{\delta_{k,j}} \left[\delta_{\eta,\mu} - 3 \frac{(\eta_k - \eta_s)(\mu_k - \mu_s)}{|\vec{r}_k - \vec{r}_s + \epsilon|^2} \right], \end{aligned}$$

where $\eta, \mu = x, y, z$, and $k, j = 1, \dots, N$.

C. Symplectic diagonalization and canonical quantization

Hereafter we utilize the frame F_3 that rotates at the frequency ω_r . Hence, we are allowed to drop $H_R(\mathbf{0}, \mathbf{r}_0)$ in Eq. (22) and the full Hamiltonian reduces to the $6N \times 6N$ -matrix $H_R(\omega_r) = \mathbf{d}\tilde{H}_R\mathbf{d}^\top/2$.

In order to perform the canonical quantization, we have first to transform the classical Hamiltonian $H_R(\omega_r)$ in canonical form. A transformation $S : (\mathbf{p}, \mathbf{q}) \rightarrow (\mathbf{P}, \mathbf{Q})$ is canonical when the condition $S\mathbb{J}S^\top = \mathbb{J}$ is satisfied, where $\mathbb{J} = i \bigoplus_{i=1}^{3N} \hat{\sigma}^y$ [40]. Since the Hessian matrix \tilde{H}_R is real and positive definite, Williamson's theorem [41] guarantees that

$$S\tilde{H}_RS^\top = W = \begin{pmatrix} \omega_1 & & & \\ & \omega_1 & & \\ & & \dots & \\ & & & \omega_{3N} \\ & & & & \omega_{3N} \end{pmatrix}, \quad (23)$$

where ω_k are real and positive numbers $\forall k = 1, \dots, 3N$, and W is called the ‘‘Williamson form’’ of \tilde{H}_R .

Given that, we can recast the classical Hamiltonian as

$$H_R(\omega_r) = \frac{1}{2} \sum_{k=1}^{3N} \omega_k \Lambda_{2k-1}^2 + \frac{1}{2} \sum_{k=1}^{3N} \omega_k \Lambda_{2k}^2, \quad (24)$$

where the new coordinates are determined by the transformation $\mathbf{\Lambda}^\top = (S^{-1})^\top \mathbf{d}^\top$. For the sake of simplicity, hereafter, we use the definitions $Q_k := \Lambda_{2k-1}$ and $P_k := \Lambda_{2k} \forall k = 1, \dots, 3N$. Thus, the Hamiltonian reduces to

$$H_R(\omega_r) = \frac{1}{2} \sum_{k=1}^{3N} \omega_k (Q_k^2 + P_k^2), \quad (25)$$

that is, a sum of uncoupled harmonic oscillators.

Similarly to Sec. II A, we perform the canonical quantization by promoting Q_k, P_k to operators such that $[\hat{Q}_k, \hat{P}_s] = i\delta_{k,s}$. Besides this, we introduce the operators $\hat{a}_k = (\hat{Q}_k + i\hat{P}_k)/\sqrt{2}$, $\hat{a}_k^\dagger = (\hat{Q}_k - i\hat{P}_k)/\sqrt{2}$ with $[\hat{a}_k, \hat{a}_s^\dagger] = \delta_{k,s}$. Hence, the quantized Hamiltonian is simply given by

$$\hat{H}_R(\omega_r) = \sum_{k=1}^{3N} \omega_k \left(\hat{a}_k^\dagger \hat{a}_k + \frac{1}{2} \right), \quad (26)$$

and we note that the eigenvalues ω_k are dimensionless.

Finally, we rewrite the coupling between the ions and the inhomogeneous laser field. The displacement of the ion from its equilibrium position can be written as

$$\hat{d}_j = \frac{1}{\sqrt{2}} \sum_{k=1}^{3N} A_{k,j}^* \hat{a}_k + A_{k,j} \hat{a}_k^\dagger \quad (27)$$

with $A_{kj} = S_{2k-1,j} + iS_{2k,j}$, and where j is an odd integer [see the definition of the vector \mathbf{d} after Eq. (22)]. Then, the matter-field interaction has the following expression

$$\begin{aligned} \hat{V} &= \sum_{j=1}^N [\vec{q}_j \cdot \vec{f}_j(t)] \hat{\sigma}_j^z = \sum_{j=0}^{N-1} \hat{\sigma}_{j+1}^z \sum_{n=1}^3 \mathcal{F}_{3j+n}(t) \hat{d}_{2(n+3j)-1} \\ &= \sum_{k=1}^{3N} \alpha_k^* \hat{a}_k + \alpha_k \hat{a}_k^\dagger, \end{aligned} \quad (28)$$

where $\mathcal{F} = (f_{1,x}, f_{1,y}, f_{1,z}, \dots, f_{N,x}, f_{N,y}, f_{N,z})$, and

$$\alpha_k = \frac{1}{\sqrt{2}} \sum_{j=0}^{N-1} \hat{\sigma}_{j+1}^z \sum_{n=1}^3 \mathcal{F}_{3j+n}(t) A_{k,2(n+3j)-1}. \quad (29)$$

Thus the full Hamiltonian is: $\hat{H} = \hat{H}_R(\omega_r) + \hat{V} = \sum_k \hat{H}_k$, where $\hat{H}_k = \omega_k \left(\hat{a}_k^\dagger \hat{a}_k + \frac{1}{2} \right) + \alpha_k^* \hat{a}_k + \alpha_k \hat{a}_k^\dagger$.

D. Two-qubit phase gate

The time evolution of a phonon mode state, governed by the Hamiltonian \hat{H}_k , and a generic two-qubit state is

$$|\Psi_k; \Phi_{\text{qbit}}(t)\rangle = e^{-i\phi_k(t)} \hat{\mathcal{D}}[\beta_k(t)] e^{-i\hat{H}_k^0} |\Psi_k; \Phi_{\text{qbit}}(0)\rangle, \quad (30)$$

where $\hat{\mathcal{D}}[\beta_k(t)]$ is the displacement operator [42], $\beta_k(t) = -i \int_0^t ds \alpha_k(s) e^{i\omega_k(s-t)}$, and $\hat{H}_k^0 = \omega_k \left(\hat{a}_k^\dagger \hat{a}_k + \frac{1}{2} \right)$.

In order to disentangle the external dynamics due to the phonons and the internal dynamics of the qubit states at the end of the gate operation, $t = \tau_g$, the following condition has to be satisfied [39]

$$\mathcal{I}_k = \frac{1}{\sqrt{\omega_k}} \int_0^{\tau_g} dt e^{i\omega_k t} \alpha_k(t) = 0 \quad \forall k. \quad (31)$$

This condition, however, is more general than the adiabatic elimination we performed in Sec. II B, whose aim was to highlight the difference in the accumulated two-particle phases among the most common quantum gate schemes based on pushing forces with off-resonant lasers.

The necessary lateral force on the j -th and k -th ion, $|\vec{f}_j| = |\vec{f}_k| = \mathcal{A}_P \hbar \omega_{xy} \cos(\nu t) e^{-t^2/\tau_g^2} / |\vec{r}_j^0 - \vec{r}_k^0|$, is determined by setting the dimensionless parameter \mathcal{A}_P to achieve a π phase between the chosen pair of qubits. Then the fidelity is given by

$$F = \min_{\Phi'_{\text{qbit}}} \left\{ \text{Tr}_{\text{ph}} \left[\langle \Phi'_{\text{qbit}} | \hat{U}(t) (\hat{\rho}_T(0) \otimes |\Phi_{\text{qbit}}\rangle \langle \Phi_{\text{qbit}}|) \hat{U}^\dagger(t) | \Phi'_{\text{qbit}} \rangle \right] \right\} = \min_{\pm} \prod_k \exp \left[-\frac{\mathcal{A}_P^2}{4} \left(\frac{|\mathcal{I}_k^{(j_1)} \pm \mathcal{I}_k^{(j_2)}|^2}{1 - e^{-\hbar\omega_k/k_B T}} \right) \right], \quad (32)$$

where $\hat{U}(t)$ is the unitary evolution operator defined through Eq. (30), $\hat{\rho}_T(0)$ is the initial (canonical) density operator of the phonon modes at temperature T , $|\Phi_{\text{qbit}}\rangle$ is the initial two-qubit state, and

$$|\Phi'_{\text{qbit}}\rangle = \sum_{\epsilon_1, \epsilon_2=0}^1 (-1)^{\epsilon_1 \epsilon_2} c_{\epsilon_1, \epsilon_2} |\epsilon_1\rangle |\epsilon_2\rangle \quad (33)$$

is the desired logical target state we aim to attain. The integral $\mathcal{I}_k^{(j_q)}$ for $q = 1, 2$ is given in Eq. (31) where the apex (j_q) refers to the ion we are considering, that is, $j = j_q$ in the sum of Eq. (29).

Since we aim to achieve $\tau_g \ll 2\pi/\omega_r$, we outline the following program: Firstly, we analyze the dependence of ω_r on the total angular momentum P_θ . This is achieved by fixing a priori a value of P_θ and then by determining the equilibrium configuration of the crystal, namely the positions and momenta of each ion (the most difficult part of the program). Since the crystal is a rigid body, it holds $p_{\theta_k} = mr_k^2 \dot{\theta}_k + er_k A_\theta(r_k) = mr_k^2 (\omega_r + \omega_c/2)$ [35], and from this relation the rotation frequency is extracted. Such an analysis allows us to find the smallest value of ω_r such that $\beta < \beta_c = 0.665/\sqrt{N}$ is fulfilled, that is, a 2D Wigner crystal configuration [35]. Then we choose the value of both ω_c and ν in order to achieve high gate fidelity for a wide range of temperatures.

The determination of the classical ground state is a multidimensional minimization constrained problem for which no deterministic and efficient algorithm is known. Here we used a variant of the Metropolis [43] and the multidimensional constrained Newton algorithm like the one of Ref. [44]. The first method allows us to sample randomly the relevant phase space region by choosing a slow decay of the acceptance probability and by using several annealing cycles. We then coarse-grained the obtained annealing trajectories into intervals, and we employed, for the lowest energy configuration on each interval, a Newton algorithm, which is very efficient in finding a local minimum provided that the initial value is already very close. We have checked the reliability of our numerical energy minimization for $P_\theta = 0$, that is $\omega_r = 2\omega_c$, by comparing the results of Ref. [44] for the minimal excitation frequency for several numbers N of ions.

We investigated the robustness of the modulated-carrier phase gate against temperature for a moderate number of ions $N = 30$ and $\alpha_z = 0.70$. In Fig. 2 the dependence of the crystal rotation frequency on the total canonical angular momentum is showed, whereas in Fig. 3 the gate infidelity for different values of the ratio τ_g/τ_r is displayed. The results of Fig. 3 refer to $P_\theta = 4000 \ell_s^2 m \omega_c$, for which we obtain the smallest value of $|\omega_r|$ in Fig. 2. Beside this, we have for such a choice $\beta = 3.4 \times 10^{-4}$,

whereas $\beta_c = 0.12$, that is, a stable 2D hexagonal lattice configuration. Given that, Fig. 3 shows that in order to reduce by a factor 10 the ratio τ_g/τ_r the fast modulation frequency ν of the force has to be (roughly) enhanced by a factor 10 as well. We also remark, that the three lines in Fig. 3 show an infidelity that is smaller for large gate operation times. The goal of the plot is to show how the modulation frequency increases when the ratio τ_g/τ_r is reduced for an infidelity smaller than 10^{-4} . Of course, by carefully tuning ν one can easily get a smaller infidelity for faster gates.

In the inset (left corner - top) the result of the gate infidelity for a cyclotron frequency 100 times higher is showed, that is, the same 7.608 MHz of the experiment of Ref. [28]. Here there are two important features to be highlighted: firstly, the gate fidelity is more robust for a wide range of temperatures with respect to the previous case where $\omega_c/(2\pi) = 76.08$ kHz has been considered. On the other hand, already for $\tau_g/\tau_r = 0.1$, the frequency ν is on the order of hundreds of MHz. In the inset on the right (bottom) we show the gate infidelity again for the $\omega_c = 7.608$ MHz but for a smaller modulation frequency $\nu = 2.4$ MHz that lies in the gap between the two bands of different radial modes (the so called $\vec{E} \times \vec{B}$ and cyclotron modes. See also Fig. 5). In this scenario $\tau_g/\tau_r = 10$ and therefore a co-rotating laser beam is required. In conclusion we see that for $\omega_z \sim \omega_c/\sqrt{2}$ if we desire to avoid the employment of a co-rotating laser beam the only possible way is to achieve very high frequencies for the modulation of the state dependent force.

Alternatively, one can consider a smaller value of α_z , which basically shifts upwards the graph of Fig. 2, that is, by displacing the minimum of the $|\omega_r|$ closer to zero for large values of P_θ . This is the situation depicted in Fig. 4 for $N = 30$, and $\alpha_z = 0.02$. Here it is possible to achieve gate operation times on the order of few μs with significantly smaller values of the modulation frequency. In the figure ν lies in the gap among axial and radial modes (see Fig. 5). Furthermore with $\tau_g/\tau_r = 6 \times 10^{-3}$ we do not need a co-rotating laser beam. This result is quite interesting since it works in a range of parameters that are currently employed in experiments (e.g., [31]). Finally we also note that in this scenario $\omega_{xy} \gg \omega_z$, which is opposite to the requirement we identified in the case of larger α_z when $2\omega_r = \omega_c$. We note, however, that ω_{xy} is not the actual radial frequency when $\omega_c \neq 2\omega_r$. Indeed, as shown in Eq. (1), the centrifugal potential (i.e., $-m\omega^2 r^2/2$) modifies the confinement. Let us write $\omega_r = (\omega_c - \delta\omega)/2$, where $\delta\omega > 0$. Then by substituting such definition into the second line of (1) we obtain an effective radial frequency given by: $\omega_{xy}^{\text{eff}} = \frac{1}{2} \sqrt{\omega_c^2 - \delta\omega^2 - 2\omega_z^2}$. With the parameters of Fig. 4 we get $\omega_{xy}^{\text{eff}}/(2\pi) = 31.47$ kHz which

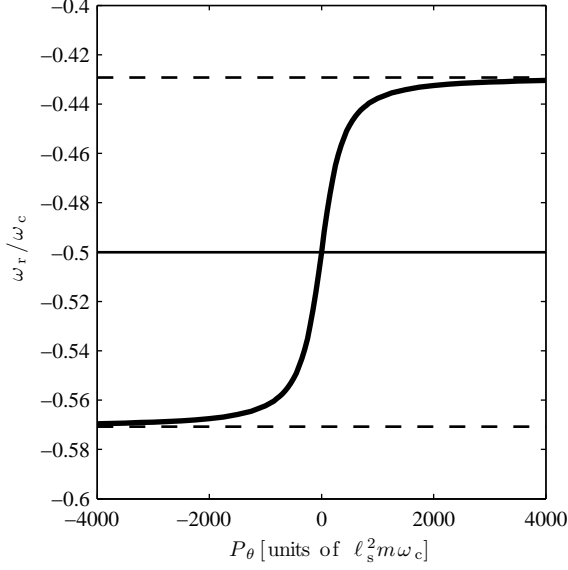


FIG. 2. (Color online). Ratio ω_r/ω_c vs. total angular momentum P_θ for $\alpha_z = 0.7$ and $N = 30$. For $P_\theta = 0$ we retrieve the well-known limit $\omega_r = 2\omega_c$, in which there is no magnetic field in the rotating frame.

is significantly smaller than ν_z (~ 152 kHz), and therefore the 2D lattice configuration is ensured. This fact is also confirmed by $\beta = 4 \times 10^{-2} < \beta_c$.

Now, let us examine what is the required laser power in order to realize the gate and investigate the influence of scattered photons on the gate performance. A pair of narrow-waist ($\leq 2\mu\text{m}$) adjacent laser beams in the standing-wave configuration produces the necessary force to be applied to each ion. Beside this, because of the tight focusing it reduces spontaneous emission and laser power. Following the treatment of Ref. [34], an estimate of the needed laser power to realize the logical gate is given by

$$P = \mathcal{A}_P \frac{\omega_{xy} \Delta \hbar \kappa^2 w^2 \sin^2(\gamma/2)}{3\Gamma |\vec{r}_i^0 - \vec{r}_j^0|}. \quad (34)$$

Here $\Delta = \omega_L - \omega_A$ is the detuning, that is, the difference between the laser and the relevant atomic transition frequencies, Γ is the linewidth of the transition, $\kappa = 2\pi/\lambda_L$ is the wave number with the laser wavelength $\lambda_L = 2\pi c/\omega_L$, c is the speed of light, w is the size of the beam waist, and γ is the angle between the κ vectors of the two laser beams (see also Fig. 1). Additionally, we can estimate the influence of photon scattering on the gate fidelity as: $F_{\text{scat}} = e^{-N_{\text{phot}}}$, where the number of scattered photons in the standing-wave configuration is given by

$$N_{\text{phot}} \approx \frac{\sqrt{2}\pi^3 \epsilon_0 c m^2 w^2 \omega_{xy}^4 |\vec{r}_i^0 - \vec{r}_j^0|^3}{3e^2 \lambda_L P} \sin\left(\frac{\gamma}{2}\right). \quad (35)$$

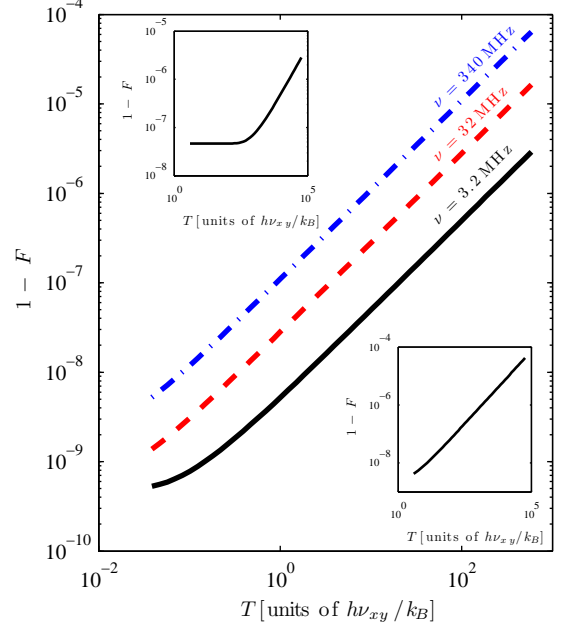


FIG. 3. (Color online). Infidelity vs. temperature for $\alpha_z = 0.7$, $N = 30$, and $P_\theta = 4 \times 10^3 \ell_s^2 m \omega_c$. Parameters: $\nu_c = \omega_c/(2\pi) = 76.08$ kHz, $\nu_{xy} = \omega_{xy}/(2\pi) = 5.38$ kHz, $\nu_z = \omega_z/(2\pi) = 53.26$ kHz, and $\nu_r = \omega_r/(2\pi) = 32.75$ kHz. The black (solid) line corresponds to $\tau_g/\tau_r = 10^{-1}$ ($\tau_g = 3\mu\text{s}$), the red (dashed) line to $\tau_g/\tau_r = 10^{-2}$ ($\tau_g = 0.3\mu\text{s}$), and the blue (dashdot) line to $\tau_g/\tau_r = 10^{-3}$ ($\tau_g = 0.03\mu\text{s}$), with $\tau_r = 2\pi/\omega_r$. The inset (on the left corner - top) provides the infidelity for $\tau_g/\tau_r = 10^{-1}$ ($\tau_g = 0.03\mu\text{s}$) with $\nu_c = 7.61$ MHz as in Ref. [28], $\nu = 300$ MHz, $\nu_{xy} = 537.97$ kHz, $\nu_z = 5.33$ MHz, and $\nu_r = 3.27$ MHz. The inset (on the right corner - bottom) illustrates, for the same trapping parameters as for the former inset but with $\nu = 2.4$ MHz, the infidelity for $\tau_g/\tau_r = 10$ ($\tau_g = 3\mu\text{s}$). Such modulation frequency ν lies within the gap among radial and $\vec{E} \times \vec{B}$ phonon modes (see Fig. 5).

As the last two formulae show, by adjusting γ we can reduce the required laser power, but at the expenses of a larger number of scattered photons, and therefore of a worsening of the gate performance.

IV. MODULATED AND STATE-DEPENDENT DIPOLE FORCE

In order to realize our quantum phase gate, $|\epsilon_1, \epsilon_2\rangle \rightarrow e^{i\theta_{\epsilon_1\epsilon_2}} |\epsilon_1, \epsilon_2\rangle$ with $\epsilon_{1,2} = 0, 1$, we have to engineer the θ_{kj} phases in θ (see also Sec. II). It is natural to demand that the desired value of θ is obtained with the smallest possible value of the applied force (i.e., laser power) or, alternatively, in the shortest possible time. This is equivalent to maximize θ by maximizing the effect of each θ_{kj} . This happens when the phases θ_{01} and θ_{10} have the opposite sign with respect to the phases θ_{00} and θ_{11} . Such condition is met when the applied force to the j -th ion

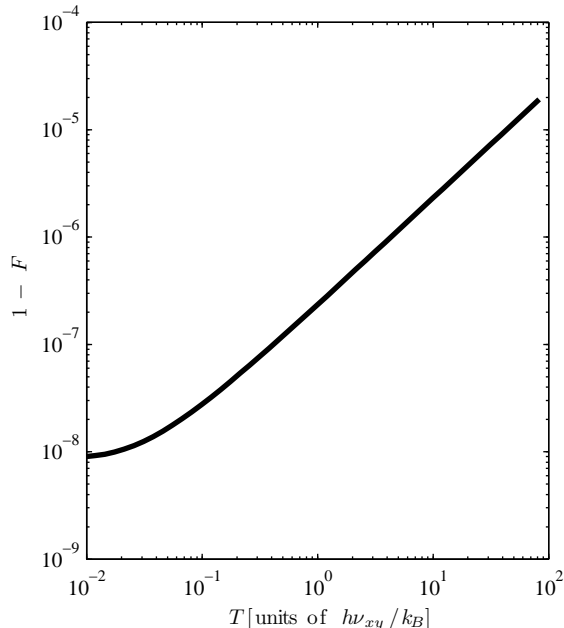


FIG. 4. (Color online). Infidelity vs. temperature for $\alpha_z = 0.02$, $N = 30$, and $P_\theta = 1.3 \times 10^5 \ell_s^2 m \omega_c$. Parameters: $\nu_c = 7.61$ MHz, $\nu_{xy} = 3.80$ MHz, $\nu_z = 152.16$ kHz, and $\nu_r = 1.65$ kHz (see text for more details).

satisfies the relation

$$\vec{f}_j^{(0)} = -\vec{f}_j^{(1)}. \quad (36)$$

Additionally, a necessary condition for the implementation of a modulated-carrier quantum phase gate is that the mean force acting on each ion (respectively each of the modes) has to be zero over τ_g , that is, we have to fulfill Eq. (31). Such a requirement can be accomplished by making the modulation time symmetric around the center of the envelope of the laser pulse. To this aim, we impose the further condition on the force:

$$\int_0^\tau dt \vec{f}_j^{(k)}(t) = 0 \quad \forall k = 0, 1, \quad (37)$$

where $\tau = 2\pi/\nu$ is one period of the modulation. With such a condition we obtain a (fast) sinusoidal modulation of the force. Experimentally, this can be achieved, for example, with an acousto-optical modulator, which can vary the frequency of the laser light very quickly.

A. Energy shifts

In table I we provide for some ion species the energy splitting between the $P_{1/2}$ and $P_{3/2}$ levels in the absence of an external magnetic field together with the maximal value of magnetic field B_Z , under which the (normal)

Atom/Ion	$\Delta E/\hbar$ (THz)	B_Z (T)	B_{PB} (T)
Be II	1.239	7.043	28.170
Mg II	17.249	98.070	392.286
Ca II	41.985	238.711	954.845
Na I	3.242	18.410	73.651

TABLE I. Energy splitting among the $P_{1/2}$ and $P_{3/2}$ levels without external the magnetic field (second column from the left). In the third and fourth columns (from the left) the maximal and minimal value of the external magnetic field, which fix respectively the upper and lower bound for the Zeeman and Paschen-Back regimes, are given.

Zeeman limit can be applied, and the minimal value B_{PB} above which we enter in the Paschen-Back regime. As we can gather from the table, the higher the atomic number of the ion (or neutral atom) is, the larger ΔE and the limits B_Z , B_{PB} . For instance, for the infidelity results we showed in the previous section, the corresponding magnetic field at $\omega_c = 7.608$ MHz are: $B = 4.5$ T and $B = 12$ T for Beryllium and Magnesium, respectively. These are also the values used in current experiments. Thus, for all alkaline-earth-metal atoms the Zeeman regime applies, and therefore $\hat{H}_B = \frac{\mu_B}{\hbar} g_J \hat{J}_z B_z$ well describes the interaction of an ion with the external magnetic field. Here g_J is the Landé factor [45] and the nuclear contribution has been neglected ($g_I \sim 10^{-3}$). Besides, since the external magnetic field has a strength of few Tesla, the ionic hyperfine structure can be also neglected. Additionally, we note that in the Paschen-Back regime the transitions from the energy (split) ground state (S -level) to the one of the excited levels (P) are identical for both ground levels when the ion is illuminated with a laser beam of a given polarization and frequency. Consequently, the dipole force (see Sec. IV B) would be the same for both states, and therefore it would not be possible in such a regime to have state-dependent forces. Instead, this is not the case for the broken degeneracy of the S and P levels due to the Zeeman effect (see Fig. 6).

Finally, we note that given the selection rule $s - s' = 0$ on the quantum number of the spin operator, optical transitions between the two levels of $S_{1/2}$ are not allowed. This fact reduces the possibility of undesired flips among the qubit pair, and therefore decoherence and dephasing mechanisms are strongly suppressed. Henceforth, we shall consider the lower energy level of $S_{1/2}$ as the logical state $|0\rangle$, whereas the upper one as $|1\rangle$.

B. Dipole force and dipole matrix elements

The dipole force is produced by an intensity gradient of the laser beam illuminating the atom, which is far detuned from the relevant atomic transition, whose levels are ac-Stark shifted. Such an energy shift creates an additional potential for the particle. For a two-level atom and in the large detuning limit $\Delta \gg |\Omega|$, the dipole force

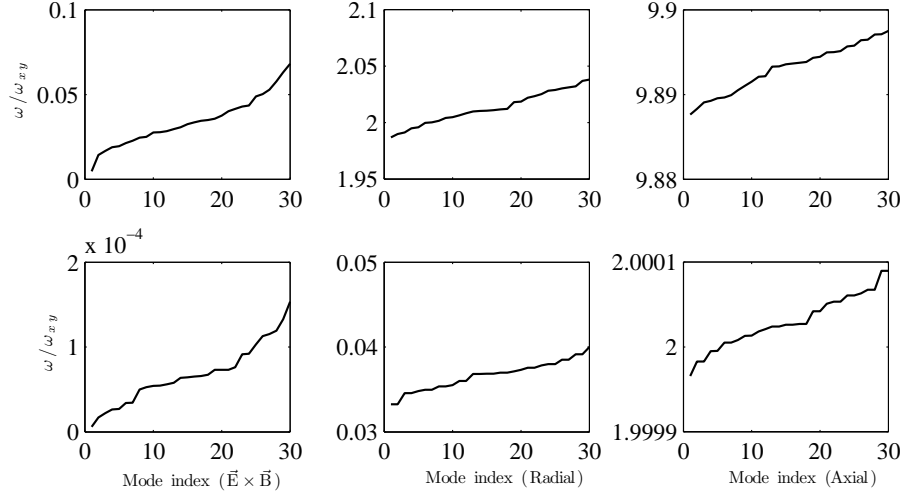


FIG. 5. (Color online). Modes for the parameters considered in Fig. 3 (top row, $\alpha_z = 0.70$, $P_\theta = 4 \times 10^3 \ell_s^2 m \omega_c$) and Fig. 4 (bottom row, $\alpha_z = 0.02$, $P_\theta = 1.3 \times 10^5 \ell_s^2 m \omega_c$).

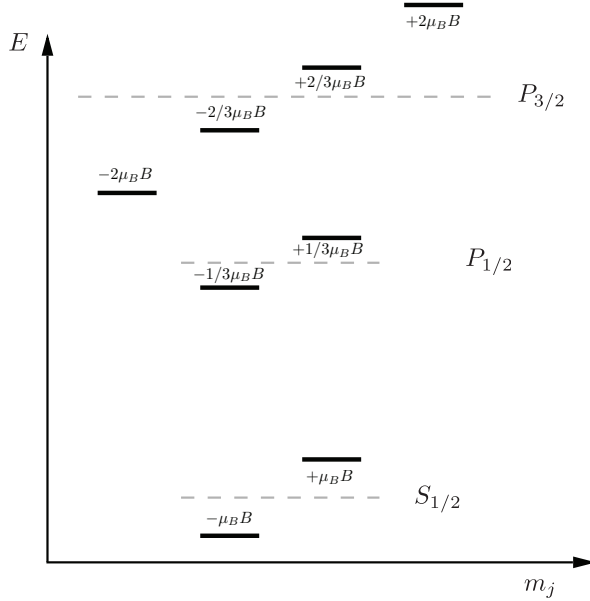


FIG. 6. (Color online). Energy shifts due to the Zeeman effect vs. the m_j quantum number. The distances among the energy levels are not in scale.

on the lower energy level reads

$$\vec{f} = -\frac{\hbar}{4\Delta} \nabla |\Omega(t, \vec{r})|^2, \quad (38)$$

where the Rabi frequency $\Omega(t, \vec{r})$ on the atomic transition is given by

$$\hbar\Omega = -\vec{d}_{ab} \cdot \vec{\mathcal{E}}(\vec{r}, t) = -|\vec{d}_{ab}| \mathcal{E}_0 \chi(\vec{r}, t), \quad (39)$$

whereas the laser is assumed to be a classical light field. Here \vec{d}_{ab} represents the matrix element of the dipole moment operator for the transition $|a\rangle \equiv |j=1/2; m_j\rangle \rightarrow |b\rangle \equiv |j=1/2, 3/2; m_j\rangle$ for a given polarization of the electric field $\vec{\mathcal{E}}$ with strength \mathcal{E}_0 , and $\chi(\vec{r}, t)$ is the spatial and temporal pulse shape.

The bare (unshifted) detunings are then defined as: $\delta_{D_1} = \omega_{L_1} - \omega_{D_1}$ and $\delta_{D_2} = \omega_{L_2} - \omega_{D_2}$, where ω_{L_1} and ω_{L_2} are the laser frequencies. In addition, in order to reduce the probability of unwanted photon scattering processes, we require that

$$|\mu_B B| \ll |\delta_{D_1}| \ll \Delta E \quad |\mu_B B| \ll |\delta_{D_2}| \ll \Delta E. \quad (40)$$

In table II we provide the expressions of the state dependent forces for all polarizations of the laser field. Since $j = 1/2$ for all relevant transitions, hereafter, for the sake of simplicity, we shall denote the reduced matrix element by $\mathcal{M}_{D_1} = \mathcal{M}_{1/2, 1/2}$ and $\mathcal{M}_{D_2} = \mathcal{M}_{1/2, 3/2}$, where $\mathcal{M}_{jj'} := \langle j, m_j \| e\hat{r} \| j', m'_j \rangle$.

C. Different laser configurations

As it is evident from the table II, using only a laser pulse either on the D_1 transition line or on the D_2 one it is not possible to fulfill the condition (36). To this aim we need a second laser pulse (see Fig. 7 on the left) with a different detuning from the first pulse. In this section we discuss several combinations of the laser polarization in order to satisfy both (36) and (37).

1. Pulses with the same polarization

In this case we first generate two laser pulses with different frequencies but with the same σ^- polarization, as

Polarization	$\vec{f}^{(0)} (D_1)$	$\vec{f}^{(1)} (D_1)$	$\vec{f}^{(0)} (D_2)$	$\vec{f}^{(1)} (D_2)$
σ^-	0	$-\frac{\mathcal{M}_{D_1}\mathcal{E}_0^2\nabla\chi^2(\vec{r},t)}{2\hbar(3\delta_{D_1}+4\mu_B B/\hbar)}$	$-\frac{\mathcal{M}_{D_2}\mathcal{E}_0^2\nabla\chi^2(\vec{r},t)}{4\hbar(\delta_{D_2}+\mu_B B/\hbar)}$	$-\frac{\mathcal{M}_{D_2}\mathcal{E}_0^2\nabla\chi^2(\vec{r},t)}{4\hbar(3\delta_{D_2}+5\mu_B B/\hbar)}$
π	$\frac{\mathcal{M}_{D_1}\mathcal{E}_0^2\nabla\chi^2(\vec{r},t)}{4\hbar(2\mu_B B/\hbar-3\delta_{D_1})}$	$-\frac{\mathcal{M}_{D_1}\mathcal{E}_0^2\nabla\chi^2(\vec{r},t)}{4\hbar(3\delta_{D_1}+2\mu_B B/\hbar)}$	$\frac{\mathcal{M}_{D_2}\mathcal{E}_0^2\nabla\chi^2(\vec{r},t)}{2\hbar(\mu_B B/\hbar-3\delta_{D_2})}$	$-\frac{\mathcal{M}_{D_2}\mathcal{E}_0^2\nabla\chi^2(\vec{r},t)}{2\hbar(3\delta_{D_2}+\mu_B B/\hbar)}$
σ^+	$\frac{\mathcal{M}_{D_1}\mathcal{E}_0^2\nabla\chi^2(\vec{r},t)}{2\hbar(4\mu_B B/\hbar-3\delta_{D_1})}$	0	$\frac{\mathcal{M}_{D_2}\mathcal{E}_0^2\nabla\chi^2(\vec{r},t)}{4\hbar(5\mu_B B/\hbar-3\delta_{D_2})}$	$\frac{\mathcal{M}_{D_2}\mathcal{E}_0^2\nabla\chi^2(\vec{r},t)}{4\hbar(\mu_B B/\hbar-\delta_{D_2})}$

TABLE II. Dipole forces for all polarizations of the laser fields and internal (logical) states.

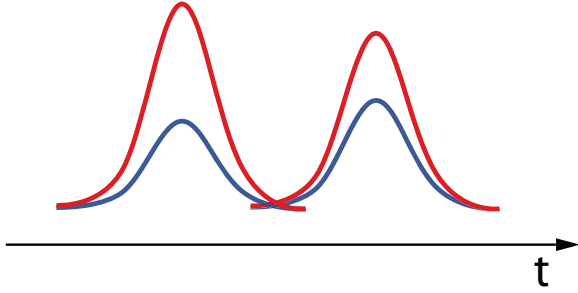
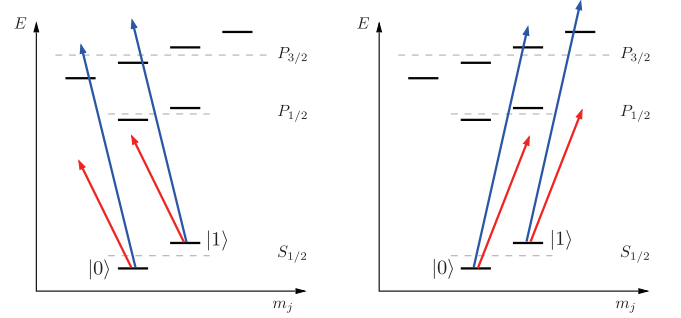


FIG. 7. (Color online). Sketch of the pulse sequence in order to design the necessary dipole forces to implement the modulated-carrier phase gate. The upper lines are red detuned, whereas the lower lines are blue detuned. In the figures the time is in arbitrary units.

FIG. 8. (Color online). Modulated-carrier gate with the same polarization of the laser fields: σ^- -polarized (left), and σ^+ -polarized (right). The distances among the energy levels are not in scale.

in Fig. 8, which corresponds to the first sequence of pulses (on the left) in Fig. 7. Such a configuration of lasers yields the following state-dependent forces:

$$\begin{aligned}\vec{f}^{(1)} &= -\frac{\mathcal{M}_{D_1}\mathcal{E}_{01}^2\nabla\chi^2(\vec{r},t)}{2\hbar(3\delta_{D_1}+4\mu_B B/\hbar)} - \frac{\mathcal{M}_{D_2}\mathcal{E}_{02}^2\nabla\chi^2(\vec{r},t)}{4\hbar(3\delta_{D_2}+5\mu_B B/\hbar)}, \\ \vec{f}^{(0)} &= -\frac{\mathcal{M}_{D_2}\mathcal{E}_{02}^2\nabla\chi^2(\vec{r},t)}{4\hbar(\delta_{D_2}+\mu_B B/\hbar)}.\end{aligned}\quad (41)$$

To simplify the notation we make the following replacements: $\mathcal{X}_{D_i} = \mathcal{M}_{D_i}\mathcal{E}_{0i}^2\nabla\chi^2(\vec{r},t)$ and $\mathcal{B} = \mu_B B/\hbar$, where \mathcal{E}_{0i} refers to the electric field strength of either the D_1 ($i = 1$) or D_2 ($i = 2$) line. Thus, in order to fulfill (36), we have to solve the equation

$$\frac{\mathcal{X}_{D_2}}{\delta_{D_2} + \mathcal{B}} + \frac{\mathcal{X}_{D_2}}{3\delta_{D_2} + 5\mathcal{B}} + \frac{2\mathcal{X}_{D_1}}{3\delta_{D_1} + 4\mathcal{B}} = 0. \quad (42)$$

This can be resolved for both the intensities or the detunings, so one of them can be considered as a given parameter. For the σ^+ -polarization we obtain an analogue equation:

$$\frac{\mathcal{X}_{D_2}}{\delta_{D_2} - \mathcal{B}} + \frac{\mathcal{X}_{D_2}}{3\delta_{D_2} - 5\mathcal{B}} + \frac{2\mathcal{X}_{D_1}}{3\delta_{D_1} - 4\mathcal{B}} = 0. \quad (43)$$

As an example, we solve equation (43), for instance, for the intensities, and we obtain

$$\frac{\mathcal{X}_{D_1}}{\mathcal{X}_{D_2}} = \frac{(4\mathcal{B} - 3\delta_{D_1})(2\delta_{D_2} - 3\mathcal{B})}{(\delta_{D_2} - \mathcal{B})(3\delta_{D_2} - 5\mathcal{B})}. \quad (44)$$

Such a solution, however, fulfills only the condition (36) but not the one given by Eq. (37). To this aim we need an additional two-pulse sequence, as showed in Fig. 7 on the right. Such two pulses can have different strengths of intensities and detunings, but they must have the same spatial and temporal profile $\chi(\vec{r},t)$ of the first sequence. Again, we get, if we solve with respect to the intensities, a solution like the one given in Eq. (44), which in general will be different from the solution (44) for the first sequence of pulses. With such solution we can then easily satisfy also the mean zero force condition (37) by adjusting the ratios of either the intensities or the detunings.

In Fig. 9 we display a simple example that shows how to achieve the necessary laser pulse sequence. We modulate the intensities of the blue (b) and red (r) detuned

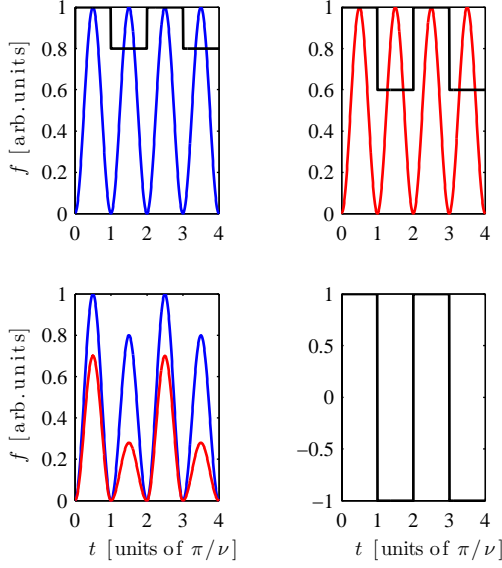


FIG. 9. (Color online). Designed laser modulation forces in order to fulfill both (37) and (36). The blue detuned laser intensity with a superimposed square wave signal (top-left) and similarly for the red detuned one (top-right). The resulting signals are depicted on the bottom-left, whereas switching of polarization is given on the bottom-right.

laser signals like $I^{b(r)}(t) = I_0^{b(r)} \sin^2(\nu t)$. The sequence starts ($t = 0$) with both lasers with σ^+ -polarization and an intensity ratio $R_+ = I_0^b/I_0^r$ given by Eq. (44). Then, at time $t = \pi/\nu$, the polarization of the two laser fields is changed to σ^- with another intensity ratio given by $R_- = I_0^b/I_0^r$. The ratio R_- will differ from R_+ , since in general the dipole moments are different for the two polarizations. Thus, by changing the polarization at each minimum of the laser intensity and by choosing the proper ratio R_{\pm} we are able to fulfill the condition (37). In order to satisfy the condition (36) we have to design furthermore the ratio of the two successive pulses. This is done by multiplying the two intensities $I^{b(r)}(t)$ with square wave signals which are displayed in Fig. 9 (top) by the black lines. The resulting pulses are showed in Fig. 9 (bottom-left) whose polarization state is depicted on the right lower corner. This procedure ensures that both the conditions (37) and (36) are fulfilled.

2. Pulses with the different polarization

The situation in which the laser beams have different polarization is depicted in Fig. 10. If we illuminate the ion with red detuned and σ_+ polarized light and with a blue detuned and σ_- beam (Fig. 10 on the left) we have the following state-dependent forces

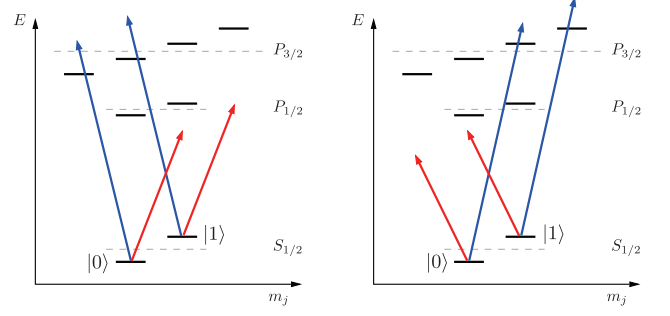


FIG. 10. (Color online). Modulated-carrier gate with different polarization of the laser fields. The distances among the energy levels are not in scale.

$$\begin{aligned} \vec{f}^{[1]} &= -\frac{\mathcal{M}_{D_2} \mathcal{E}_0^2 \nabla \chi^2(\vec{r}, t)}{4\hbar(3\delta_{D_2} + 5\mu_B B/\hbar)}, \\ \vec{f}^{[0]} &= \frac{\mathcal{M}_{D_1} \mathcal{E}_0^2 \nabla \chi^2(\vec{r}, t)}{2\hbar(4\mu_B B/\hbar - 3\delta_{D_1})} - \frac{\mathcal{M}_{D_2} \mathcal{E}_0^2 \nabla \chi^2(\vec{r}, t)}{4\hbar(\delta_{D_2} + \mu_B B/\hbar)}, \end{aligned} \quad (45)$$

whereas for the inverted polarization sequence (Fig. 10 on the right) we have

$$\begin{aligned} \vec{f}^{[1]} &= \frac{\mathcal{M}_{D_2} \mathcal{E}_0^2 \nabla \chi^2(\vec{r}, t)}{4\hbar(\mu_B B/\hbar - \delta_{D_2})} - \frac{\mathcal{M}_{D_1} \mathcal{E}_0^2 \nabla \chi^2(\vec{r}, t)}{2\hbar(3\delta_{D_1} + 4\mu_B B/\hbar)}, \\ \vec{f}^{[0]} &= \frac{\mathcal{M}_{D_2} \mathcal{E}_0^2 \nabla \chi^2(\vec{r}, t)}{4\hbar(5\mu_B B/\hbar - 3\delta_{D_2})}. \end{aligned} \quad (46)$$

Both the schemes with the same and with different polarization have the drawback that the transition to the excited level $P_{3/2}$ couples both the ground states of $S_{1/2}$, and therefore producing an additional force that has to be compensated with another laser beam. Apart from the technical difficulty of putting another laser beam, such a beam would also enhance the probability of promoting an ion to an excited level of $P_{3/2}$. Such excitation would cause an additional error during the course of the gate because of spontaneous emission. Indeed, the ion could decay either in the other qubit state or even worst, such as for the D -levels in calcium, in another metastable state, which would be useless for the purposes of QIP.

Given that, in order to avoid such scenario, we can make still use of the scheme illustrated in Fig. 10, but by avoiding the coupling to the $P_{3/2}$ manifold, as it is showed in Fig. 11. Here, however, we couple the ground state $S_{1/2}$ to only the manifold $P_{1/2}$. The pulse sequences are then the same as previously described for the other scheme. The detuning from the $P_{1/2}$ manifold, however, has to be carefully chosen, that is, it has to be much smaller than the energy difference among the $P_{1/2}$ and $P_{3/2}$ levels and much larger than $\mu_B B$. Hence, such variant works well for sufficiently small magnetic fields.

In principle there are other possible arrangements either by keeping the frequencies of the laser beams con-

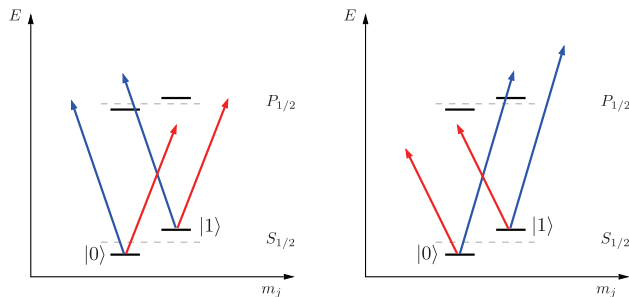


FIG. 11. (Color online). Variant of the modulated-carrier gate with different polarization of the laser fields. The distances among the energy levels are not in scale.

stant or by keeping constant their intensities. Such combinations rely also on the technical feasibility in an experimental setup. An important requirement for the design of such state-dependent forces is, however, the switch of the field polarization, which has to be very fast in order to fulfill the condition set by the Eq. (37), as it is also shown in the example of Fig. 9(d). This can be experimentally accomplished with Pockels cells, which can be used to manipulate the polarization and the phase of the laser.

V. CONCLUSIONS

In this work we have analyzed in detail the implementation of the modulated-carrier gate presented for the first time in Ref. [30]. Firstly, we presented the underlying idea of the modulated-carrier gate and we provided details of the calculations that were only briefly mentioned in Ref. [30]. In that analysis the frame of reference rotates at the same frequency of the crystal rotation, whose frequency was set to $\omega_c = 2\omega_r$. Within this setting the minimal coupling term in the many-body Hamiltonian vanishes. Such approach allows a straightforward canonical quantization of the many-body Hamiltonian, which reduces to a sum of $3N$ independent harmonic oscillators. Even though this situation greatly simplifies the numerical analysis it does not permit to fulfill the condition $\omega_r\tau_g/(2\pi) \ll 1$, which would avoid the utilization of a co-rotating laser and therefore simplifying the experimental realization of the proposed quantum hardware. We thus have analyzed the situation in which $\omega_c \neq 2\omega_r$. Within this scenario it is no longer possible to remove the minimal coupling term in the Hamiltonian of the Coulomb crystal. Nevertheless, by utilizing the Williamson theorem for positive definite matrices, we were able to diagonalize the classical many-body Hamiltonian, whose normal modes are a combination of both the position and momentum variables. As a consequence, we were able to perform the canonical quantization. The resulting (quantized) Hamiltonian is again given by a

sum of independent harmonic oscillators. In this new situation, however, the matter-field interaction, responsible of the push on the ion, depends on both conjugate “position” and “momentum” operators. We proceeded further on by analyzing the performance of the quantum phase gate and we showed its robustness for a wide range of experimentally accessible temperatures. Importantly, we were able to demonstrate that such robustness is also displayed for a wide range of ratios τ_g/τ_r , therefore allowing to reduce up to three orders of magnitude the gate operation time compared to the previous analysis [30]. The drawback is that one has to enhance the modulation frequency ν up to hundreds of MHz in order to speed up the gate operation. We found, however, that by reducing the ratio ω_z/ω_c , at large values of angular momentum it is possible to achieve small rotation frequencies such that $\omega_r\tau_g/(2\pi) \ll 1$ is fulfilled and high fidelity, for a broad range of temperatures, can be obtained with few MHz of modulation frequency. This result is quite promising since it has been attained with a cyclotron frequency that is used in current experiments.

Finally, we have provided a complete description for the design of the necessary forces to be applied on the ions in order to accomplish the desired quantum computation scheme. To this aim, we have analyzed the experimentally relevant region of external magnetic field. For all earth-alkali-metal ion species normally used in currents experiments the normal Zeeman effect provides, with good approximation, the right description of the energy shifts of the S and P levels. In addition, we have also analyzed several possible laser configurations and for each one we discussed advantages as well as drawbacks and, in some cases, we suggested alternative solutions.

Further investigations of such a quantum computing proposal may rely on further optimization of both the force modulation together with a reduced gate operation time and its robustness against optimal pulse distortions [46]. This can be achieved by means of quantum optimal control techniques. Beside this, a detailed analysis, similar to Ref. [9], in order to characterize and quantify all types of errors coming from the quantum dynamics, especially due to nonlinearities in the ion-pushing force, will be pursued in future investigations.

ACKNOWLEDGMENTS

We are grateful to J. J. Bollinger for his critical reading of the manuscript. J.B. acknowledges G. De Chiara and E. Kajari for helpful discussions, and A.N. useful correspondence with E. Pagani on symplectic transformations. We acknowledge financial support from the EU Integrated Project AQUTE, PICC (T.C.), the Deutsche Forschungsgemeinschaft within the Grant No. SFB/TRR21 (A.N.,T.C.), the Marie Curie Intra European Fellowship (Proposal Nr. 236073, OPTIQUOS) within the 7th European Community Framework Programme (A.N.), the Forschungsbonus of the University

of Ulm and of the Ulmer Universitäts-gesellschaft (A.N.), the Spanish Ministry of Science and Innovation (Con-

solider Ingenio 2010 “QOIT”, QNLP FIS2007-66944), and the European Science Foundation (EUROQUAM “Cavity-Mediated Molecular Cooling”) (J.B.).

-
- [1] E. Charron, E. Tiesinga, F. Mies, and C. Williams, *Phys. Rev. Lett.*, **88**, 077901 (2002).
 - [2] J. P. Palao and R. Kosloff, *Phys. Rev. Lett.*, **89**, 188301 (2002).
 - [3] T. Calarco, U. Dorner, P. S. Julienne, C. J. Williams, and P. Zoller, *Phys. Rev. A*, **70**, 012306 (2004).
 - [4] P. Treutlein, T. W. Hänsch, J. Reichel, A. Negretti, M. A. Cirone, and T. Calarco, *Phys. Rev. A*, **74**, 022312 (2006).
 - [5] E. Charron, M. A. Cirone, A. Negretti, J. Schmiedmayer, and T. Calarco, *Phys. Rev. A*, **74**, 012308 (2006).
 - [6] S. Montangero, T. Calarco, and R. Fazio, *Phys. Rev. Lett.*, **99**, 170501 (2007).
 - [7] F. Motzoi, J. M. Gambetta, P. Rebentrost, and F. K. Wilhelm, *Phys. Rev. Lett.*, **103**, 110501 (2009).
 - [8] S. Safaei, S. Montangero, F. Taddei, and R. Fazio, *Phys. Rev. B*, **79**, 064524 (2009).
 - [9] U. V. Poulsen, S. Sklarz, D. Tannor, and T. Calarco, *Phys. Rev. A*, **82**, 012339 (2010).
 - [10] A. M. Steane, *Phys. Rev. A*, **68**, 042322 (2003).
 - [11] E. Knill, *Phys. Rev. A*, **71**, 042322 (2005).
 - [12] D. Leibfried, B. DeMarco, V. Meyer, D. Lucas, M. Barrett, J. Britton, W. M. Itano, B. Jelenković, C. Langer, T. Rosenband, and D. J. Wineland, *Nature*, **422**, 412 (2003).
 - [13] J. Benhelm, G. Kirchmair, C. F. Roos, and R. Blatt, *Nat. Phys.*, **4**, 463 (2008).
 - [14] S. Gulde, M. Riebe, G. P. T. Lancaster, C. Becher, J. Eschner, H. Häffner, F. Schmidt-Kaler, I. L. Chuang, and R. Blatt, *Nature*, **421**, 48 (2003).
 - [15] J. Chiaverini, J. Britton, D. Leibfried, E. Knill, M. D. Barrett, R. B. Blakestad, W. M. Itano, J. D. Jost, C. Langer, R. Ozeri, T. Schätz, and D. J. Wineland, *Science*, **308**, 997 (2005).
 - [16] D. Kielpinski, C. Monroe, and D. J. Wineland, *Nature*, **417**, 709 (2002).
 - [17] D. Stick, W. K. Hensinger, S. Olmschenk, M. J. Madsen, K. Schwab, and C. Monroe, *Nat. Phys.*, **2**, 36 (2006).
 - [18] R. Folman, P. Krüger, D. Cassettari, B. Hessmo, T. Maier, and J. Schmiedmayer, *Phys. Rev. Lett.*, **84**, 4749 (2000).
 - [19] J. Reichel, W. Hänsel, and T. W. Hänsch, *Phys. Rev. Lett.*, **83**, 3398 (1999).
 - [20] M. Oskin, F. T. Chong, and I. L. Chuang, *IEEE Comp.*, **35**, 79 (2002).
 - [21] J. I. Cirac, P. Zoller, H. J. Kimble, and H. Mabuchi, *Phys. Rev. Lett.*, **78**, 3221 (1997).
 - [22] E. Brion, K. Mølmer, and M. Saffman, *Phys. Rev. Lett.*, **99**, 260501 (2007).
 - [23] A. Steane, C. F. Roos, D. Stevens, A. Mundt, D. Leibfried, F. Schmidt-Kaler, and R. Blatt, *Phys. Rev. A*, **62**, 042305 (2000).
 - [24] G. Chen, D. A. Church, B.-G. Englert, C. Henkel, B. Rohwedder, M. O. Scully, and M. S. Zubairy, *Quantum Computing Devices: Principles, Designs, and Analysis* (Chapman & Hall/CRC Taylor & Francis Group, Boca Raton, 2006).
 - [25] F. Anderegg, C. F. Driscoll, C. H. E. Dubin, and T. M. O’Neil, *Phys. Plasmas*, **17**, 055702 (2010).
 - [26] T. B. Mitchell, J. J. Bollinger, D. H. E. Dubin, X.-P. Huang, W. M. Itano, and R. H. Baughman, *Science*, **282**, 1290 (1998).
 - [27] D. J. Wineland, J. Dalibard, and C. Cohen-Tannoudji, *J. Opt. Soc. Am. B*, **9**, 32 (1992).
 - [28] T. B. Mitchell, J. J. Bollinger, W. M. Itano, and D. H. E. Dubin, *Phys. Rev. Lett.*, **87**, 183001 (2001).
 - [29] D. Porras and J. I. Cirac, *Phys. Rev. Lett.*, **96**, 250501 (2006).
 - [30] J. M. Taylor and T. Calarco, *Phys. Rev. A*, **78**, 062331 (2008).
 - [31] M. J. Biercuk, H. Uys, A. P. VanDevender, N. Shiga, W. M. Itano, and J. J. Bollinger, *Quantum Info. and Comp.*, **9**, 920 (2009).
 - [32] J. I. Cirac and P. Zoller, *Nature*, **404**, 579 (2000).
 - [33] T. Calarco, J. I. Cirac, and P. Zoller, *Phys. Rev. A*, **63**, 062304 (2001).
 - [34] M. Šašura and A. M. Steane, *Phys. Rev. A*, **67**, 062318 (2003).
 - [35] D. H. E. Dubin and T. M. O’Neil, *Rev. Mod. Phys.*, **71**, 87 (1999).
 - [36] P. K. Gosh, *Ion traps* (Clarendon Press, Oxford, 1995).
 - [37] C. Itzykson and J. B. Zuber, *Quantum Field Theory* (McGraw-Hill International Book Co., New York, 1980).
 - [38] J. J. García-Ripoll, P. Zoller, and J. I. Cirac, *Phys. Rev. Lett.*, **91**, 157901 (2003).
 - [39] J. J. García-Ripoll, P. Zoller, and J. I. Cirac, *Phys. Rev. A*, **71**, 062309 (2005).
 - [40] A. Fasano and S. Marmi, *Analytical Mechanics* (Oxford University Press, New York, 2006).
 - [41] J. Williamson, *Am. J. Math.*, **58**, 141 (1936).
 - [42] C. W. Gardiner and P. Zoller, *Quantum Noise*, Springer Series in Synergetics (Springer, Heidelberg, 2004).
 - [43] N. Metropolis, A. W. Rosenbluth, M. N. Rosenbluth, A. H. Teller, and E. Teller, *J. Chem. Phys.*, **21**, 1087 (1953).
 - [44] V. A. Schweigert and F. M. Peeters, *Phys. Rev. B*, **51**, 7700 (1995).
 - [45] H. A. Bethe and E. E. Salpeter, *Quantum Mechanics of One- and Two-Electron Atoms* (Oxford University Press, New York, 1957).
 - [46] A. Negretti, R. Fazio, and T. Calarco, arXiv:1007.2405.